FLUID DYNAMIC TREATMENT OF THIXOTROPIC DEBRIS FLOWS AND AVALANCHES

HUBERT CHANSON [1] and PHILIPPE COUSSOT [2]

[1]Dept of Civil Engineering, The University of Queensland, Brisbane QLD 4072, Australia
(Tel: +61-7-3365-4163, Fax: +61-7-3365-4599, e-mail: h.chanson@uq.edu.au)
[2]Laboratoire des Matériaux et Structures du Génie Civil, Unité Mixte de Recherche
(LCPC-ENPC-CNRS), 2 allée Kepler, 77420 Champs-sur-Marne, France

Abstract

Some forms of mud flows and debris flows exhibit a non-Newtonian thixotropic behaviour, and this study describes a basic study of dam break wave with thixotropic fluid. Theoretical considerations were developed based upon a kinematic wave approximation of the Saint-Venant equations down a prismatic sloping channel and combined with the thixotropic rheological model of Coussot et al. (2002). The analytical solution of basic flow motion and rheology equations predicts three basic flow regimes depending upon the fluid properties and flow conditions, including the initial degree of jamming of the fluid. The present work is the first theoretical analysis combining successfully the basic principles of unsteady flow motion with a thixotropic fluid model, which was verified with systematic laboratory experiments.

Keywords : Debris flow; Thixotropy; Dam break wave; Kinematic wave; Analytical solution

1. INTRODUCTION

In natural mudflows, the interstitial fluid made of clay and water plays a major role in the rheological behaviour of the complete material. Since clay-water suspensions have often been considered as thixotropic yield stress fluids, it is likely that thixotropy plays a role in some cases of natural events. Thixotropy is the characteristic of a fluid to form a gelled structure over time when it is not subjected to shearing and to liquefy when agitated. A thixotropic fluid appears as a non-Newtonian fluid exhibiting an apparent yield stress and an apparent viscosity that are functions of both the shear intensity and the current state(s) of structure of the material. Under constant shear rate, the apparent viscosity of a thixotropic fluid changes with time until reaching equilibrium. To date, it is essentially the yielding character of non-Newtonian fluid behaviour which has been taken into account for modelling either steady, slow spreading and rapid transient free surface flows (Liu and Mei 1989, Coussot 1997, Laigle and Coussot 1997). There is a need to explore the interplay of the yielding and thixotropic characters of mud and debris flows.

This work describes a basic study of dam break wave with thixotropic fluid. Such a highly unsteady flow motion has not been studied to date with thixotropic fluid, despite its practical applications : e.g., mudflow release, concrete tests including L-Box and J-Ring for self-consolidating concrete testing, preparation of industrial paints. Herein a theoretical analysis is

developed. One-dimensional equations are developed yielding analytical solutions of the problem, and results are discussed. It is the purpose of this paper to fill a void in this field, to compare theoretical developments with physical modelling results, and to present new compelling conclusions regarding highly unsteady flow motion of thixotropic fluids.

1.1 FLUID RHEOLOGY

For a Newtonian fluid, the shear stress acting in a direction is proportional to the velocity gradient $\partial V/\partial y$ in the normal direction. The constant of proportionality is the dynamic viscosity. For some sediment-laden flows with large concentrations of fine particles, the Bingham plastic model is more appropriate (e.g. Wan and Wang 1994). For thixotropic fluids, various models have been proposed to describe their behaviour (e.g. Mewis 1979). Most have a similar structure consisting of an apparent viscosity function of the shear rate $\partial V/\partial y$ and of some structure parameter(s) associated with some kinetic equation(s) giving the time evolution of the structure parameter(s) as function(s) of time and shear rate. Coussot et al. (2002) proposed a simple model to describe the rheological properties of a thixotropic fluid:

$$m = m_o * (1 + l^n) \quad (1)$$

$$\frac{\partial l}{\partial t} = \frac{1}{q} - a * \frac{\partial V}{\partial y} * l \quad (2)$$

where μ_o, n, θ and α are four constant parameters for a given fluid, and μ is the apparent viscosity of the thixotropic fluid defined as $\mu = \tau/\partial V/\partial y$ with τ being the shear stress, V the velocity and y the normal direction. Equations (1) and (2) imply that the degree of jamming of thixotropic fluid can be represented by a single parameter λ describing the instantaneous state of fluid structure. The degree of jamming of the fluid λ could represent the degree of flocculation of clays or the fraction of particles in potential wells for colloidal suspensions (Coussot et al. 2002). One advantage of this model is that flow simulations do not require the determination of a solid-liquid limit like other yield stress models. The model is capable to predict qualitatively the trends of fluid behaviours, as well as quantitative properties under steady and unsteady states (e.g. Roussel et al. 2004).

2. THEORETICAL TREATMENT

A dam break wave is the flow resulting from a sudden release of a mass of fluid in a channel (Fig. 1A). For a sloping wide rectangular channel, Hunt (1984) developed a complete kinematic wave solution of the Saint-Venant equations based upon the basic equations :

$$\frac{\partial d}{\partial t} + \frac{\partial (V * d)}{\partial x} = 0 \quad \text{Continuity equation (3)}$$

$$V = \sqrt{\frac{8 * g}{f}} * d * S_o \quad \text{Kinematic wave equation (4)}$$

where d is the flow depth or fluid thickness measured normal to the invert, V is the depth-average velocity, t is the time, x is the coordinate in the flow direction positive downstream, f is the Darcy friction factor and S_o is the bed slope ($S_o = \sin\theta_b$) (Fig. 1A). The combination of continuity and momentum equations may be rewritten as :

$$\frac{D\,d}{Dt} = 0 \tag{5}$$

along the forward characteristic trajectory :

$$\frac{d\,x}{dt} = \frac{3}{2} * \sqrt{\frac{8 * g}{f} * S_o * d} \tag{6}$$

where D/Dt characterises the absolute differentiation operator (Hunt 1984, Chanson 2004). The free-surface profile must further satisfy the conservation of mass :

$$\int_{x=-L}^{X_S} d * dx = \frac{1}{2} * H_{dam} * L * \cos\theta_b = \frac{1}{2} * d_o * L \tag{7}$$

where L is the reservoir length, H_{dam} is the dam height, d_o is the initial reservoir height measured normal to the chute invert and X_S is the wave front position (Fig. 1A). The dam removal is associated with the dam break wave propagation as well as a backward characteristic propagating upstream into the reservoir initially at rest. Since the propagation of the initial negative wave is relatively rapid, the complete equations of Saint Venant must be solved. The initial backward characteristic propagates in a fluid at rest (V = 0, S_f = 0) and its upstream extent is:

$$x = -\frac{1}{4} * g * S_o * t^2 \qquad \text{Initial backward characteristic} \tag{8}$$

where t is the time from dam removal. For a two-dimensional triangular reservoir, the initial backward characteristic reaches the reservoir upstream end at the time $T = \sqrt{4*L/(g*S_o)}$.

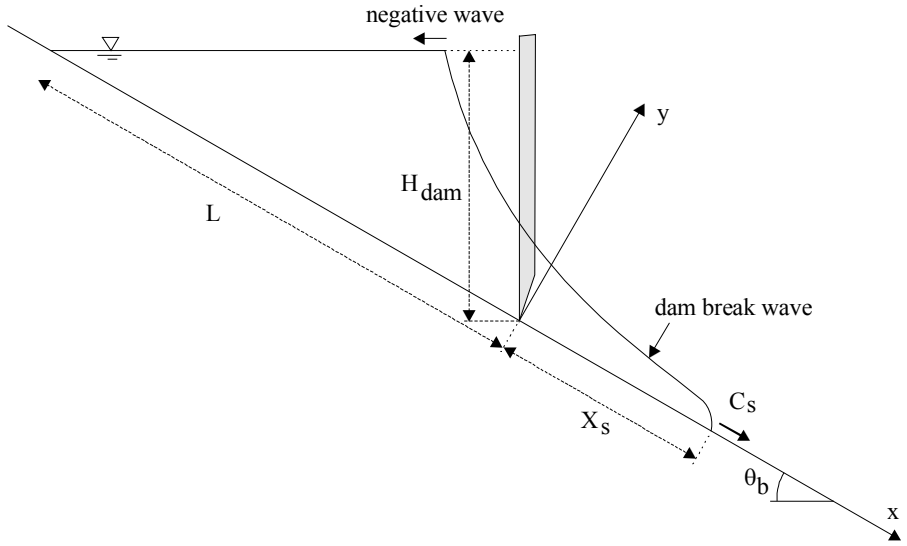

(A) Definition sketch

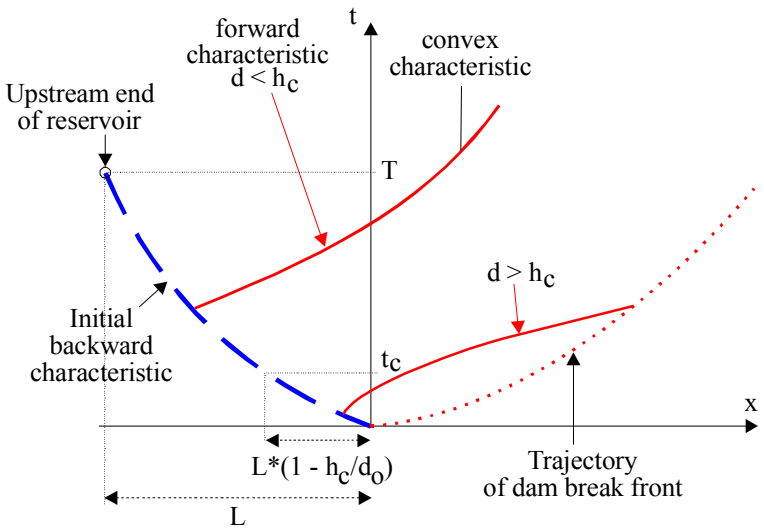

(B) Sketch of characteristic curves for a dam break wave of thixotropic fluid

Fig. 1 Dam break wave of thixotropic fluid

Using the model of Coussot et al. (2002), the rheological equations (Eq. (1) and (2)) may be approximated by assuming $\partial V/\partial y \approx V/d$ and $\tau_o = \mu * V/d$, where τ_o is the boundary shear stress and μ is the apparent fluid viscosity. The kinematic wave approximation ($S_o = S_f$) yields :

$$V = \frac{\rho * g * S_o * d^2}{\mu_o * (1 + \lambda^n)} \qquad \text{Kinematic wave approximation} \quad (9)$$

Along a characteristic trajectory, the degree of jamming of the material satisfies :

$$\frac{d\lambda}{dt} = \frac{1}{\theta} - \alpha * \frac{\rho * g * d * S_o}{\mu_o} * \frac{\lambda}{1 + \lambda^n} \qquad (10)$$

with d = constant along the forward characteristic. Combining Equations (6) and (9), the equation of the forward characteristic trajectory becomes:

$$\frac{dx}{dt} = \frac{3}{2} * \frac{\rho * g * S_o * d^2}{\mu_o * (1 + \lambda^n)} \qquad \text{Forward characteristic trajectory} \quad (11)$$

The characteristic trajectories are not straight lines since λ is a function of time and space (Fig. 1B).

2.1 DISCUSSION

Several analytical developments may be derived in particular cases, including for $\theta \rightarrow +\infty$ or for integer values of n (App. I). More generally, for $n > 1$, Equation (10) predicts different behaviours along a forward characteristic depending upon the sign of $d\lambda/dt$ and the initial degree of jamming $\lambda(t=0) = \lambda_o$. It may be rewritten as :

$$\frac{d\lambda}{dt} = F_2(\lambda) \qquad (10b)$$

Note that the function $\lambda/(1+\lambda^n)$ tends to zero for $\lambda \rightarrow 0$ and $\lambda \rightarrow +\infty$, and it has a maximum for $\lambda = \lambda_c = (n-1)^{-1/n}$. Hence the equation $F_2(\lambda) = 0$ has zero real solution, one solution λ_c or two solutions λ_1 and λ_2 depending upon the dimensionless viscosity $\mu_o/(\theta*\alpha*\rho*g*d*S_o)$. The function $F_2(\lambda)$ is

positive for $\lambda \to 0$ and $\lambda \to +\infty$. It is negative for $\lambda_1 < \lambda < \lambda_2$ when the equation $F_2(\lambda) = 0$ has two real solutions.

For a dam break down a sloping channel, Equation (10) gives at the time origin (t = 0) :

$$\left(\frac{d\lambda}{dt}\right)_{t=0} = \alpha * \frac{\rho * g * d * S_o}{\mu_o} * \left(\frac{\mu_o}{\theta * \alpha * \rho * g * d * S_o} - \frac{\lambda_o}{1 + \lambda_o{}^n}\right) \quad (12)$$

along the forward characteristic where d is constant and λ_o is the initial degree of fluid jamming. When the term inside the brackets (right handside, Eq. (12)) is positive (Case 1), $\lambda(t>0) > \lambda_o$, and, by extension, λ increases monotically towards the wave front. For large times ($t >> 1$), $d\lambda/dt$ tends to $1/\theta$ and the degree of jamming λ tends to an infinite value : i.e., complete stoppage. The result is independent of the initial degree of jamming λ_o. A similar reasoning may be developed when the term inside the brackets (right handside, Eq. (12)) is negative (Case 2), with three basic flow situations depending upon the signs of $(\lambda_o - \lambda_1)$ and $(\lambda_o - \lambda_2)$. For $(\lambda_o > \lambda_2 > \lambda_1)$, $d\lambda/dt$ is positive for $t \geq 0$ everywhere along the characteristic trajectory and λ increases monotically until complete flow stoppage. For $(\lambda_1 < \lambda_o < \lambda_2)$, $d\lambda/dt \leq 0$ at $t \geq 0$, although $d\lambda/dt$ tends to zero and λ tends to λ_1 for large times ($t >> 1$). Along a forward characteristic, the fluid flow tends to a constant viscosity behaviour ($\mu = \mu_o*(1+\lambda_1{}^n)$). For $(\lambda_o < \lambda_1 < \lambda_2)$, $d\lambda/dt \geq 0$ at $t \geq 0$. $d\lambda/dt$ tends to zero and λ tends to λ_1 for large times ($t >> 1$). The fluid flow tends again to a constant viscosity fluid behaviour ($\mu_o*(1+\lambda_1{}^n)$).

3. APPLICATION TO DAM BREAK AND AVALANCHE

Although the above discussion was developed along a forward characteristic on which the flow depth was constant, it may be extended to the sudden dam break of a finite volume reservoir. Considering a series of characteristics issued from the initial negative characteristic, the flow depth d is constant on each forward characteristic and it must satisfy : $0 \leq d \leq d_o$ (Fig. 1B). Three flow situations may occur depending upon the initial degree of fluid jamming λ_o and the ratio d_o/h_c where d_o is the initial reservoir thickness at the dam and h_c is a critical fluid thickness below which the fluid flow motion tends to complete stoppage :

$$h_c = \frac{\mu_o * (n - 1)^{1/n}}{\theta * \alpha * \rho * g * S_o} \quad (13)$$

For $d < h_c$, λ increases monotically along a forward characteristic until fluid stoppage.

Case (a) : For reservoir depths less than the characteristic fluid thickness (i.e. $d_o < h_c$), the degree of jamming of the fluid increases monotically with time on each forward characteristic until fluid stoppage. The extent of fluid flow is limited and the flow motion is relatively slow until complete stoppage. The result is independent of the initial degree of fluid jamming λ_o.

Case (b) : For larger initial reservoirs (i.e. $d_o > h_c$), each characteristic may have a different behaviour from adjacent characteristics depending upon the signs of $(\lambda_o-\lambda_1)$ and $(\lambda_o-\lambda_2)$. Typical trends are illustrated in Fig. 2, showing time-variations of dimensionless effective viscosity along a forward characteristic. Following the initial backward characteristic, the flow depth satisfies $h_c < d < d_o$ for $0 < t < t_c$ and $0 < d < h_c$ for $t_c < t < T$ where T is the time taken by the initial characteristic to reach the reservoir upstream end. On each characteristic issued from the initial negative characteristic

at $t > t_c$, the flow depth d is less than the characteristic fluid thickness h_c. The degree of fluid jamming λ increases monotically, the flow motion is relatively slow and the extent of fluid flow is limited until complete stoppage. For $\lambda_o > \lambda_2$, λ and μ increase monotically along all forward characteristics until complete stoppage (Case b1). The extent of flow motion is moderate until fluid stoppage. For $\lambda_1 < \lambda_o < \lambda_2$ (Case b2), the fluid flow tends to a constant viscosity behaviour ($\mu = \mu_o*(1+\lambda_1^n)$) with increasing time towards the wave front (Fig. 2). That is, the flow tends to a rapid motion towards the wave front. Similarly, for $\lambda_o < \lambda_1$ (Case b3), the fluid flow tends to a constant viscosity or fast motion ($\mu = \mu_o*(1+\lambda_1^n)$) towards the shock on the forward characteristics. Basically, Cases b2 and b3 tend to relatively similar flow conditions.

Case (c) : For very large initial reservoirs (i.e. $d_o >> h_c$) and an initial degree of jamming λ_o such as $\lambda_o << \lambda_2$, the fluid flows as a quasi-constant viscosity wave motion. The flow motion is relatively rapid and it will stop only when the fluid thickness becomes less than the characteristic fluid thickness h_c. The maximum extent of the wave front may be deduced from the equation of conservation of mass. Assuming that complete stoppage occurs for $d = h_c$ and that the final fluid thickness remains h_c, the continuity equation yields the final wave front position $(X_s)_{end}$:

$$(X_s)_{end} = \frac{1}{2} * \frac{\theta * \alpha * \rho * g * S_o * d_o * L}{\mu_o * (n - 1)^{1/n}} \qquad (14)$$

Equation (14) is a crude approximation assuming a two-dimensional flow. But its qualitative trends are coherent with both fluid rheological properties and flow motion equations.

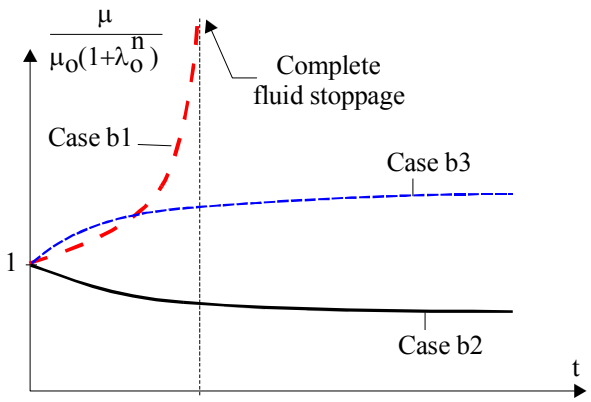

Fig. 2 Variations of dimensionless effective viscosity with increasing time along forward characteristics in a dam break wave down a sloping channel ($d_o > h_c$)

4. COMPARISON BETWEEN EXPERIMENTS AND THEORETICAL CALCULATIONS

Experiments were conducted systematically in two facilities with bentonite suspensions, using various masses of fluid M, bentonite mass concentrations C_m and rest times T_o (Chanson et al. 2004). Photographs of experiments are presented in Figure 3 and Table 1 summarises the investigated flow conditions. The results demonstrated four basic fluid flow patterns for the range of investigated flow conditions, although the present classification might be different on longer flumes. For small bentonite mass concentrations ($C_m \leq 0.15$) and

short relaxation times ($T_o \leq 30$ s), the fluid flowed rapidly down the constant-slope plate and it spilled into the overflow container (Type I). During the initial instants immediately following gate opening ($t^*\sqrt{g/d_o} < 4.1$), the flow was subjected to a very-rapid acceleration over a short period. Inertial effects were dominant leading to some form of two-dimensional "orifice" flow motion. Afterwards, the fluid flowed rapidly down the inclined chute, the flow became three-dimensional and the suspension appeared to have a very low viscosity. For intermediate concentrations and rest periods, the suspension flowed rapidly initially, as described above, decelerated relatively suddenly, continued to flow slowly for sometimes and later the flow stopped, often before the plate downstream end (Type II). Observations suggested three distinct flow periods. Immediately after gate opening, the fluid was rapidly accelerated. The flow out of the gate was quasi-two-dimensional and somehow similar to a sudden orifice flow. Then the suspension continued to flow rapidly although sidewall effects started to develop. The latter were associated with a slower front propagation at and next to the walls. Later the fluid decelerated relatively rapidly, and this was followed by a significant period of time during which the suspension continued to flow slowly before stopping ultimately. In view in elevation, the front exhibited a distinctive quasi-parabolic shape centred around the channel centreline. After stoppage, the fluid had a relatively uniform constant thickness but near the upstream end of the tail (Fig. 3A & 3B). For large mass concentrations and long rest periods, the mass of fluid stretched very-slowly down the slope, until the head separated from the tail (Type III, Fig. 3C). After separation, a thin film of suspension connected the head and tail volumes which could eventually break for long travelling distance of the head. The head had a crescent ("croissant") shape. For long rest periods (i.e. several hours), several successive packets were sometimes observed (Type IIIb). The last flow pattern (Type IV) corresponded to an absence of flow. Sometimes, a slight deformation of the reservoir, with some cracks, were observed.

Experiments showed that the conditions for the transition between flow regimes were functions of the mass concentration of bentonite suspension C_m, rest time T_o and initial mass of fluid M. A summary of observations is shown in Figure 4 for a fixed mass M. Basically the type of flow regime changed from no flow (Type IV) to a rapid flow (Type I) with increasing mass M, decreasing mass concentration C_m and decreasing rest period T_o. Figure 4 illustrates the trend in terms of mass concentration and rest period for a given mass of fluid and constant channel slope.

Theoretical fluid motion and rheology considerations yield a characteristic fluid thickness h_c below which the fluid flow motion tends to complete stoppage (Eq. (13)) and final wave front position $(X_s)_{end}$ (Eq. (14)). A comparison with experimental observations of final front locations and fluid thicknesses provides some estimate for the rheological parameters. Although the product $\theta^*\alpha$ may be estimated using either Equations (13) or (14), comparisons with experiments gave similar results. Results are summarised in Table 2 and show that the product $\theta^*\alpha$ must decrease with increasing mass concentration, thus increasing minimum apparent yield stress.

5. DISCUSSION

The physical observations of flow regimes were in remarkable agreement with theoretical considerations. In particular, exactly the same flow regimes were identified as well as same trends for the effects of the bentonite concentration and rest time. For example, theoretical considerations predict an intermediate motion with initially rapid before final fluid stoppage for intermediate mass of fluid M (i.e. $d_o/h_c > 1$) and intermediate initial rest period T_o. The theory predicts a faster flow stoppage with increasing rest period. Similarly, it shows that an increase in bentonite mass concentration, associated with an increase in the product ($\theta*\alpha$), yields a faster fluid stoppage with a larger final fluid thickness. A similar comparison between theory and physical experiments may be developed for fast-flowing motion and relatively-rapid flow stoppage situations. This qualitative agreement between simple theory and reality means that the basic physical ingredients of the rheological model and kinematic wave equations are likely to be at the origin of the observed phenomena. Interestingly the Flow Type III is the only flow pattern not predicted by theoretical considerations. It is believed that this reflects simply the limitations of the Saint-Venant equations (1D flow equations) and of the kinematic wave approximation that implies a free-surface parallel to the chute invert, hence incompatible with the Type III free-surface pattern (e.g. Fig. 3C).

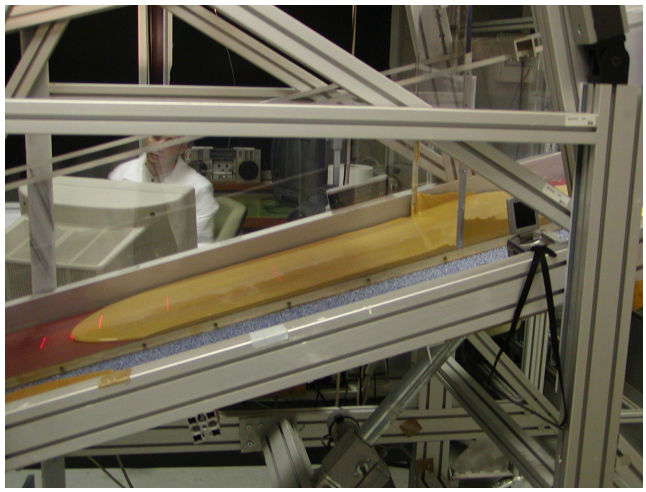

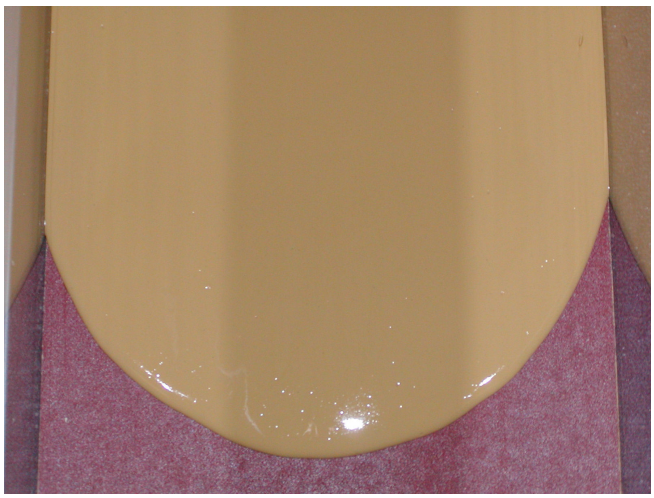

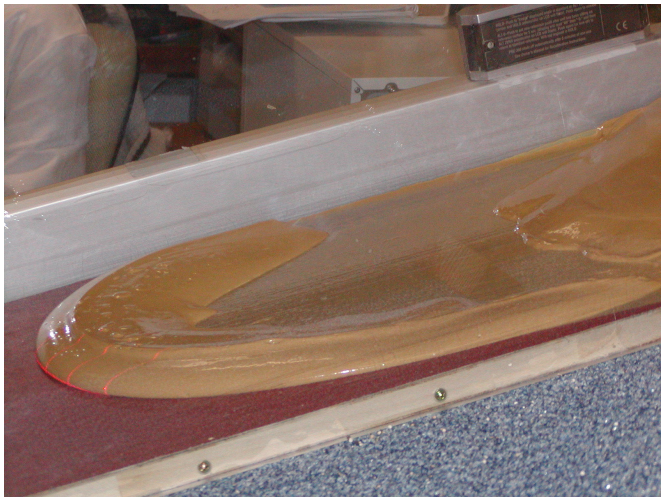

Fig. 3 Experiment with bentonite suspension (Photographs taken after fluid stoppage) - (A, Top) Flow type II, C_m = 0.15, rest period: T_o = 60 s (B, Middle) Flow type II, C_m = 0.15, T_o = 60 s, view in elevation (C, Bottom) Flow type III, C_m = 0.15, rest period: T_o = 2400 s, sideview of the head packet

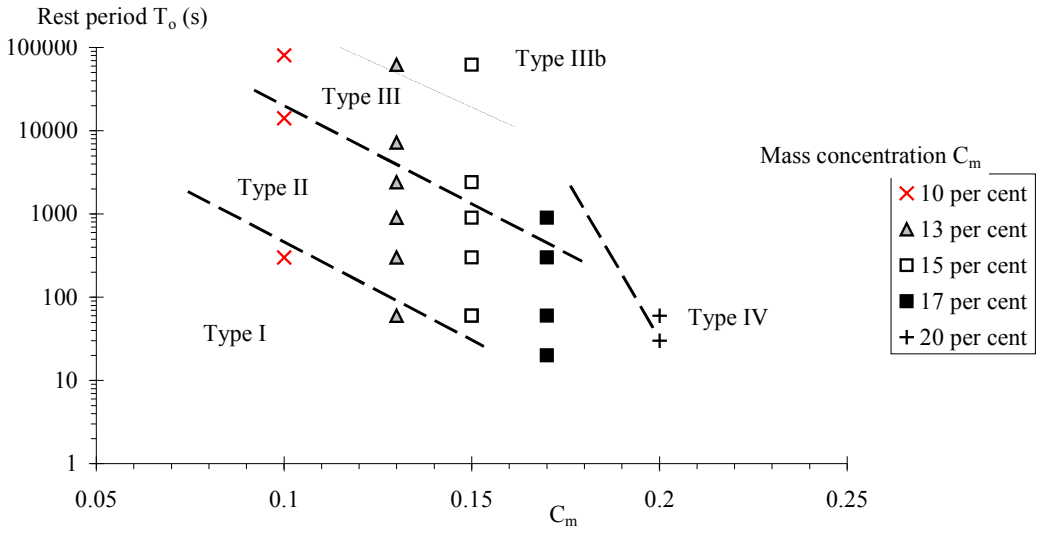

Fig. 4 Flow regime chart - Rest time T_o as function of mass concentration C_m for a given mass of fluid (M = 3.7 kg) and fixed slope ($_b$ = 15º)

Table 1. Summary of experimental flow conditions with bentonite suspensions

Facility	Slope q_b (º)	Mass concentration C_m	Initial mass M (kg)	Rest period T_o (s)	Remarks
(1)	(2)	(3)	(4)	(5)	(6)
Large flume	15.0	0.10, 0.13, 0.15, 0.17 & 0.20	1.6 to 4.1	20 sec. to 23 hours	Two-dimensional triangular reservoir. Chute length : 2.0 m. Chute width: 0.340 m.
Small plate	15.4 to 24	0.05 to 0.20	0.2 to 0.5	0 to 30 min.	Cylindrical and square moulds. Plate size: 0.8 m by 0.48 m.

Table 2. Comparison between final fluid thickness and wave front position data, and Equations (14) and (15) with bentonite suspensions ($_b$ = 15º) - Values of n and * for best data fit

C_m	kg/m^3	o Pa.s	n	* s	Remarks
(1)	(2)	(3)	(4)	(5)	(4)
0.10	1064	0.34	1.1	0.014	2 experiments (Flow types I & II).
0.13	1085	0.34	1.1	0.0032	7 experiments (Flow types I, II & III).
0.15	1100	0.34	1.1	0.0017	5 experiments (Flow types II & III).

Equations (10) and (11) may be further integrated numerically to predict time-variations of dam break wave profile, while the instantaneous locations X_s and celerity C_s of the shock front. are derived from the continuity equation (Eq. (7)). Typical results are presented in Fig. 5. Qualitatively and quantitatively, numerical calculations were in agreement with experimental

observations, but for the instants after dam removal (i.e. $t^*\sqrt{g/d_o} < 5$). Hunt (1984) showed that, for turbulent flows, the kinematic wave approximation was valid after the wave front travelled approximately four reservoir lengths downstream of the gate : i.e., $X_S/L > 4$. The assumption is not valid in the initial instants after dam break nor until the free-surface becomes parallel to the chute invert. Hunt commented however: "it is possible that an approach similar [...] could be used to route the flood downstream and that the result might be valid even for relatively small distance downstream". With thixotropic fluids, a comparison between experiments and calculations suggested that the kinematic wave approximation seemed reasonable once the wave front travelled approximately one to two reservoir lengths downstream of the gate : i.e., $X_S/L > 1$ to 2.

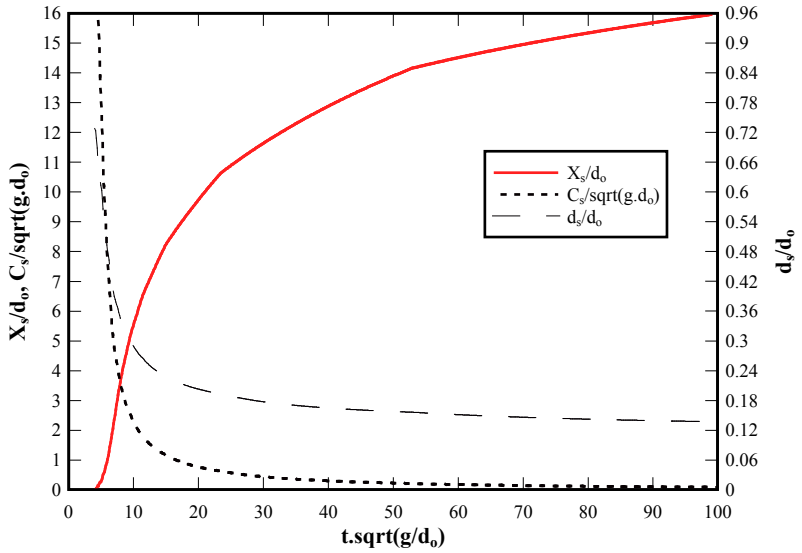

Fig. 5 Numerical calculations of dam break wave of thixotropic fluid for M = 3.8 kg, ρ =1099 kg/m^3, μ_o = 0.34, θ = 1, $\theta^*\alpha$ = 0.0017, n = 1.1, λ_o = 0.1 - Dimensionless wave front location X_S/d_o, celerity $C_S/\sqrt{g^*d_o}$ and thickness d_S/d_o

6. CONCLUSION

A basic study of dam break wave with thixotropic fluid is presented. Practical applications include self-flowing concretes, industrial paints, mud and debris flows. Theoretical considerations were developed based upon a kinematic wave approximation of the Saint-Venant equations down a prismatic sloping channel and combined with the thixotropic rheological model of Coussot et al. (2002). Theoretical results highlight three different flow regimes depedning upon the initial degree of fluid jamming λ_o and upon the ratio d_o/h_c. These flow regimes are: (1) a relatively-rapid flow stoppage for relatively small mass of fluid ($d_o/h_c < 1$) or large initial rest period T_o (i.e. large λ_o) (Cases A and B1), (2) a fast flow motion for large mass of fluid ($d_o/h_c >> 1$) (Case C), and (3) an intermediate motion initially rapid before final fluid stoppage for intermediate mass of fluid ($d_o/h_c > 1$) and intermediate initial rest period T_o (i.e. intermediate λ_o) (Cases B2 and B3). The qualitative agreement between the present theory and the experiments of Chanson et al. (2004) suggests that the

basic equations of this development (i.e. kinematic wave equation and rheology model) are likely to model correctly both fluid behaviour and flow motion.

7. APPENDIX I - ANALYTICAL SOLUTIONS OF THE METHOD OF CHARACTERISTICS TO DAM BREAK WAVE OF THIXOTROPIC FLUID

Assuming that the fluid viscosity tends to zero for infinitely high shear rate (i.e. $\mu = \mu_o * \lambda^n$), Equation (10) predicts that the degree of jamming λ increases monotically for $\lambda_o > \lambda_c$ where λ_o is the initial degree of jamming and λ_c is a characteristic degree of jamming of the fluid defined as :

$$\lambda_c = \left(\theta * \alpha * \frac{\rho * g * d * S_o}{\mu_o} \right)^{1/(n-1)} \quad \text{(I-1)}$$

Physically, for $\lambda_o > \lambda_c$, the fluid viscosity increases with increasing time along the trajectory towards the shock. Since λ and μ increase toward the wave front, the flow resistance increases and the velocity decreases. Conversely λ decreases monotically along the forward characteristic trajectory for $\lambda_o < \lambda_c$. In summary, along a forward characteristic trajectory, the fluid evolves either towards complete stoppage for $\lambda > \lambda_c$, or towards a quasi-steady flow motion ($\lambda < \lambda_c$) in which the flow resistance counter-balances exactly the gravity force component in the flow direction. (Note however that the flow resistance tends to zero, since the viscosity is zero (i.e. ideal fluid) for $\lambda = 0$.) The theory was extended to a complete dam break problem by Chanson et al. (2004).

More generally, Equation (10) may be solved analytically for integer values of n. For n = 1, the analytical solution of Equation (10) is:

$$\frac{t}{\theta} = \lambda + a*\lambda*(Ln((a-1)*\lambda - 1) - Ln\theta) - (\lambda_o + a*\lambda_o*(Ln((a-1)*\lambda_o - 1) - Ln\theta)) \quad \text{(I-2)}$$

where : $a = \alpha*\rho*g*d*S_o*\theta/\mu_o$ must be positive and greater than unity. For n = 2, the analytical solution of Equation (10) is:

$$t = \theta*\lambda + \alpha*\frac{\rho*g*d*S_o*\lambda}{\mu_o} * \frac{ArcTan\left(\frac{\lambda}{\sqrt{1 - \alpha*\frac{\rho*g*d*S_o}{\mu_o}*\theta*\lambda}}\right)}{\sqrt{\frac{1}{\theta^4} - \alpha*\frac{\rho*g*d*S_o}{\mu_o}*\lambda}} - t_o \quad \text{(I-3)}$$

where ArcTan is the inverse tangent function and t_o is a characteristic time. Further analytical solutions may be obtained for positive integer values of n assuming that all other parameters, but λ, are independent of x and t.

REFERENCES

Chanson, H. (2004). "Environmental Hydraulics of Open Channel Flows." Elsevier Butterworth Heinmann, Oxford, UK, 483 pages (ISBN 0 7506 6165 8).

Chanson, H., Coussot, P., Jarny, S., and Toquer, L. (2004). "A Study of Dam Break Wave of Thixotropic Fluid: Bentonite Surges down an Inclined plane." Report No. CH54/04, Dept. of Civil Engineering, The University of Queensland, Brisbane, Australia, June, 90 pages.

Coussot, P. (1997). "Mudflow Rheology and Dynamics." IAHR Monograph, Balkema, The Netherlands.

Coussot, P., Nguyen, A.D., Huynh, H.T., and BONN, D. (2002). "Avalanche Behavior in Yield Stress Fluids." Physics Review Letters, Vol. 88, p. 175501

Henderson, F.M. (1966). "Open Channel Flow." MacMillan Company, New York, USA.

Hunt, B. (1984). "Perturbation Solution for Dam Break Floods." Jl of Hyd. Engrg., ASCE, Vol. 110, No. 8, pp. 1058-1071.

Hunt, B. (1994). "Newtonian Fluid Mechanics Treatment of Debris Flows and Avalanches." Jl of Hyd. Engrg., ASCE, Vol. 120, No. 12, pp. 1350-1363.

Laigle, D., and Coussot, P. (1997). "Numerical Modelling of Mudflows." Journal of Hydraulic Engineering, ASCE, Vol. 123, pp. 617-623.

Liu, K.F., and Mei, C.C. (1989). "Slow Spreading of a Sheet of Bingham Fluid on an Inclined Plane." J. Fluid Mech., Vol. 207, pp. 505-529.

Mewis, J. (1979). "Thixotropy - A General Review." Jl of Non-Newtonian Fluid Mech., Vol. 6, No. 1, p. 1-20.

Roussel, N., Le Roy, R., and Coussot, P. (2004). "Thixotropy Modelling at Local and Macroscopic Scales." Jl of Non-Newtonian Fluid Mech., Vol. 117, No. 2-3, pp. 85-95.

Wan, Zhaohui, and Wang, Zhaoyin (1994). "Hyperconcentrated Flow." Balkema, IAHR Monograph, Rotterdam, The Netherlands, 290 pages.